Chapter 7

Magnetically dominated MHD bow shock flows: three-dimensional flow over a sphere

In this Chapter we present numerical simulation results of 3D MHD bow shock flows around perfectly conducting rigid spheres.

Fig. 7.1 shows a 3D visualization of a bow shock flow around a sphere with magnetically dominated uniform upstream flow (switch-on shocks occur). In the 3D flow magnetic field lines can slip over the sphere, so we are not restricted to field-aligned flow like in the 2D case, but we can consider upstream flows with an angle θ_{vB} between the magnetic field and the velocity. In the flow of Fig. 7.1 the angle $\theta_{vB} = 5°$. The upstream magnetic field is aligned with the x-axis. The xy plane is the plane going through the center of the sphere to which the upstream magnetic field and velocity vectors are parallel. The xy plane is a plane of top-bottom symmetry. Shaded density contours and magnetic field lines are shown in the xy plane, and density contours are plotted in two additional grid planes. Fig. 7.1 shows that a complex topology involving two consecutive shock fronts is obtained for this magnetically dominated bow shock flow. This topology is very different from the traditional single-front topology known from hydrodynamic bow shock flows (Fig. 2.3). The magnetically dominated flow of Fig. 7.1 shows a slightly dimpled leading shock front and a secondary shock front which is attached to the leading front and which extends well out of the xy plane. The magnetic field lines are refracted strongly at the secondary shock, which indicates that this shock is of the slow or intermediate type.

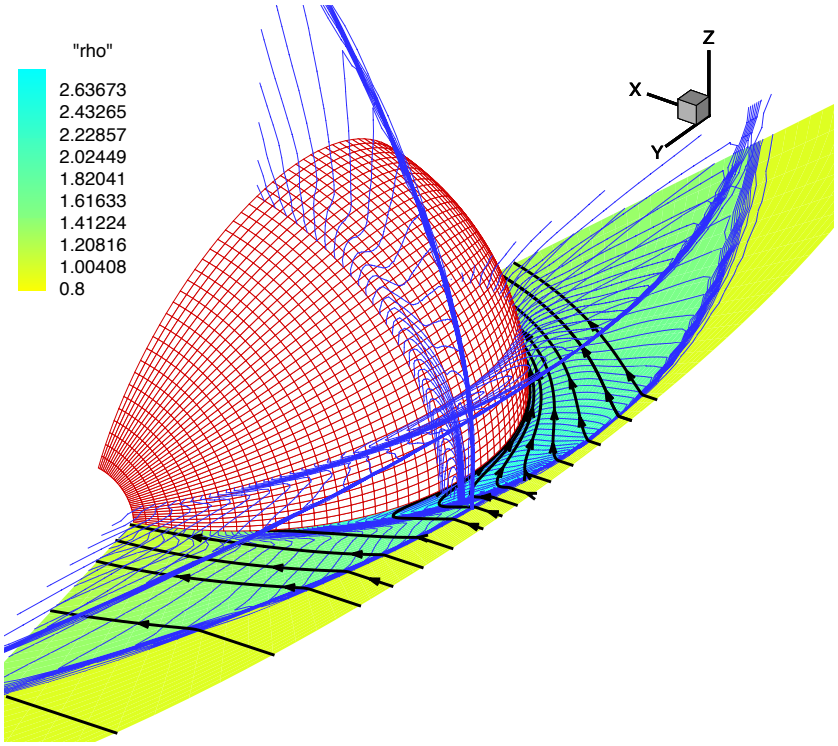

Figure 7.1: *Magnetically dominated 3D bow shock flow around a sphere with inflow* $\beta = 0.4$, $M_{Ax} = 1.49$, *and* $\theta_{vB} = 5°$. *Density contours and magnetic field lines are shown in the xy plane, which is a plane of symmetry parallel to the upstream magnetic field and velocity vectors and going through the center of the sphere. Density contours are also shown in two additional planes. In the upstream flow the magnetic field is aligned to the x-axis. The leading shock front is clearly followed by a secondary shock front, which is attached to the leading front, and which extends well out of the xy plane* ($40 \times 80 \times 40$ *grid*).

The numerical simulation results to be presented in this Chapter show that there exist two basic topologies for 3D MHD bow shock flows. For pressure-dominated upstream flows a single-front topology is obtained which is the same as the well-known topology of hydrodynamic bow shock flows. For magnetically dominated upstream flows, for which switch-on shocks occur, we find the complex bow shock topology of Fig. 7.1. This magnetically dominated bow shock topology was previously unknown.

3D MHD computations are numerically challenging and they push computer hardware performance to its limit. Therefore the 3D simulation results presented in this Chapter are less exhaustive than the 2D results presented in the previous Chapter. The 3D simulations have a rather low spatial resolution and only a limited set of parameter values has been investigated. Nevertheless, the simulation results reveal a new MHD bow shock topology which arises for all simulated bow shock flows for which the upstream flow is magnetically dominated (switch-on shocks occur), while for pressure-dominated flows the traditional single-front topology is obtained. It is confirmed by theoretical reasoning in terms of the geometrical properties of intermediate and switch-on shocks that two different 3D bow shock topologies have to exist for the magnetically dominated and the pressure-dominated regimes.

The present Chapter investigates the complex geometrical and topological phenomenology of 3D MHD bow shocks for magnetically dominated upstream parameters, in the abstract setting of stationary bow shock flows around perfectly conducting spheres. In the next Chapter we investigate observational evidence for the occurrence of such complex bow shock phenomena in space physics plasmas.

This Chapter is organized as follows. In Sec. 7.1 we present numerical simulation results which show that magnetically dominated 3D MHD bow shock flows exhibit a complex new topology. In Sec. 7.2 the special case of axi-symmetrical 3D bow shock flow over a sphere with the magnetic field aligned to the flow is considered. The stability of the symmetrical solution is discussed. In Sec. 7.3 the topology of the 3D magnetically dominated bow shock flows is explained in terms of the properties of MHD shocks. Sec. 7.4 treats transient wave phenomena which occur in the time-dependent evolution towards steady bow shock flows in 2D and 3D. We conclude briefly in Sec. 7.5.

7.1 3D bow shock flow over a sphere

7.1.1 Set-up of the simulations

In this Section we present numerical simulation results of 3D MHD bow shock flows over a sphere. We use the configuration of the simulation in Fig. 7.1. Fig. 7.2 shows the grid used for the 3D simulations. The 3D simulation code employs Cartesian xyz coordinates, but for convenience we also introduce a spherical $r\theta\phi$ coordinate system in Fig. 7.2. We place the origin O of the xyz coordinate system in the center of the sphere. The xy plane is a horizontal plane through the center of the sphere, and the xz plane is a vertical plane through the center of the sphere. In our simulations a uniform flow falls in from the left in Fig. 7.2. Generally we take the inflow magnetic field parallel to the x-axis. We align the

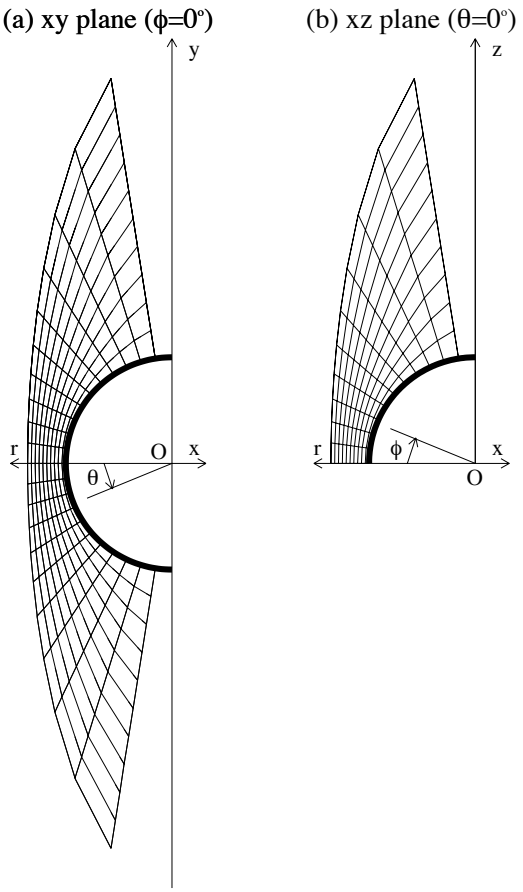

Figure 7.2: *Finite volume grid used for the 3D simulations. (a) Top view on the horizontal xy plane through the center of the sphere, which is aligned with the inflow velocity and magnetic field vectors. (b) Side view on the vertical xz plane through the center of the sphere.*

coordinate system such that $v_z = 0$ and $B_z = 0$ in the inflow. The xy plane through the sphere center is parallel to the incoming velocity and magnetic field vectors, and is thus a plane of symmetry. This symmetry allows us to restrict the simulation domain to the half-space above the xy plane. We are interested in the bow shock flow in front of the sphere, so we further restrict the simulation domain to the quadrant bordered

by the xy and yz planes. For a given point P in the simulation domain, r is the distance from P to the origin O. The angle θ is the angle between the line PO and the xz plane. The angle ϕ is the angle between the plane defined by point P and the y-axis, and the xy plane. Surfaces of constant ϕ are planes which contain the y-axis.

Fig. 7.2 shows that the simulations are performed on a stretched polar-like elliptic grid. Fig. 7.2a shows the grid in the horizontal xy plane. The y-axis is a *singular* axis in the finite volume grid, because one side plane of the finite volume hexahedrals would degenerate into a line on the y-axis. The cell volumes would become very small, and the CFL time step condition would become too restrictive. Therefore we limit our simulations to a domain $\theta \in [-90° + \alpha, 90° - \alpha]$ and $\phi \in [0°, 90° - \alpha]$, with a typical value of $\alpha = 9°$ for the constant. The simulation of Fig. 7.1 was performed on a $40 \times 80 \times 40$ grid, with 40 computational cells in the radial direction r, 80 cells in the angular direction θ, and 40 cells in the angular direction ϕ. The grid resolution is increased near interesting features of the flow by accumulating or clustering grid points. This grid accumulation is done in a dimension by dimension way.

We impose ideal wall boundary conditions at the xy plane, which is a plane of symmetry. The $\phi = 90° - \alpha$ plane satisfies free outflow boundary conditions, and the $\theta = \pm(90° - \alpha)$ surfaces are free outflow boundaries as well. The outer boundary surface in the radial direction, of ellipsoid shape, is a free inflow boundary. The spherical inner radial boundary is the perfectly conducting sphere.

The problem of uniform MHD flow over a sphere has three free parameters. Two free parameters parametrize the scales (Sec. 3.1.3). We choose the inflow plasma β and Alfvénic Mach number M_{Ax} along the magnetic field. The third parameter is the upstream angle θ_{vB} between the magnetic field and the velocity. When this angle is non-vanishing, the problem is intrinsically 3D. The corresponding hydrodynamic problem of flow over a sphere has only *one* free parameter, for instance the Mach number M, and is essentially 2D because the solution is always axi-symmetric. The general problem of ideal MHD flow around a sphere has only very partially been explored in the literature. Only limited sets of parameter values have been considered, see e.g. [174, 144].

7.1.2 Pressure-dominated 3D bow shock flows

Fig. 7.3 shows the stationary simulation result for a bow shock flow with inflow parameters $\rho = 1$, $p = 0.2$, $B = 1$ and $v = 4$, obtained on a $30 \times 60 \times 30$ grid with the second order LF scheme (Sec. 4.2.5). We align the inflow fields with the xy plane, and the magnetic field with the x-axis. The angle between the velocity and magnetic field is $\theta_{vB} = 5°$, such that the velocity has a small positive y-component. The plasma

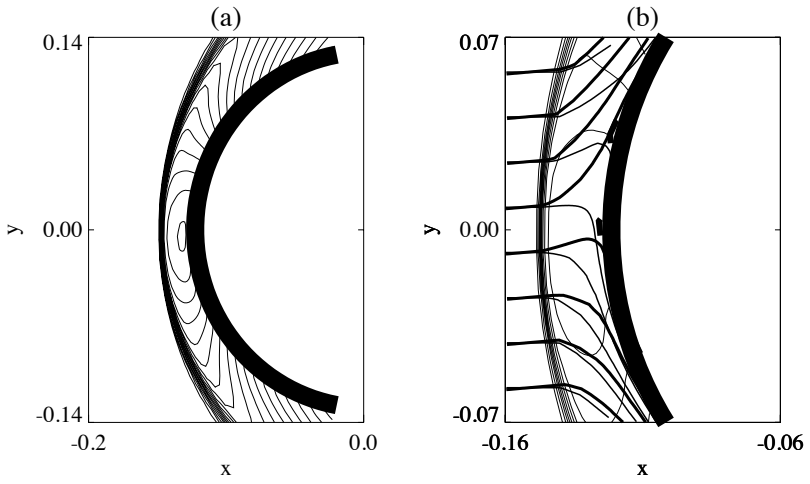

Figure 7.3: *Pressure-dominated 3D bow shock flow. (a) Density contours in the xy plane. (b) Density contours (thin solid) with streamlines (thick solid) and magnetic field lines (thin solid) in the xy plane. The two thick dots immediately in front of the sphere indicate the location of the velocity and magnetic field stagnation points* ($30 \times 60 \times 30$ *grid).*

$\beta = 0.4$, and the Alfvénic Mach number along the magnetic field lines M_{Ax}=3.98. Fig. 6.3a shows that switch-on shocks cannot arise for these parameters. The upstream flow is thus pressure-dominated.

Fig. 7.3a shows density contours in the xy plane. The bow shock solution has the traditional single-front concave-inward geometry. Fig. 7.3b shows a detailed representation of the solution near the sphere. Magnetic field lines (thin solid) come in horizontally from the left, and the incoming streamlines (thick solid) make a small angle with the magnetic field lines. Downstream of the bow shock, however, this angle is quite large at places.

It is interesting to study the location of the stagnation point in this flow. In a field-aligned flow, there is a single point where both the velocity and magnetic field strengths vanish. When the magnetic field is not aligned to the flow, points of vanishing magnetic field and velocity still exist, but those two points do generally not coincide anymore, such that there is a velocity stagnation point which is different from the magnetic stagnation point. Indeed, in the 3D bow shock flows under consideration, the streamlines and field lines which lie in the xy plane in the upstream part of the flow remain in this plane also in the downstream flow because of symmetry, such that the z components of the velocity

and the magnetic field vanish everywhere in the xy plane. In the xy plane the fluid finds its way around the sphere using the two sides (top and bottom in Fig. 7.3b), such that there necessarily is a point on the sphere boundary in the xy plane where the velocity vanishes. This velocity stagnation point is indicated by the lower one of the two thick dots in Fig. 7.3b immediately in front of the sphere. A similar reasoning can be applied to the magnetic field, resulting in the existence of a magnetic stagnation point, which is indicated by the upper thick dot in Fig. 7.3b. The simulation results thus show that the two stagnation points do not coincide.

7.1.3 Magnetically dominated 3D bow shock flows

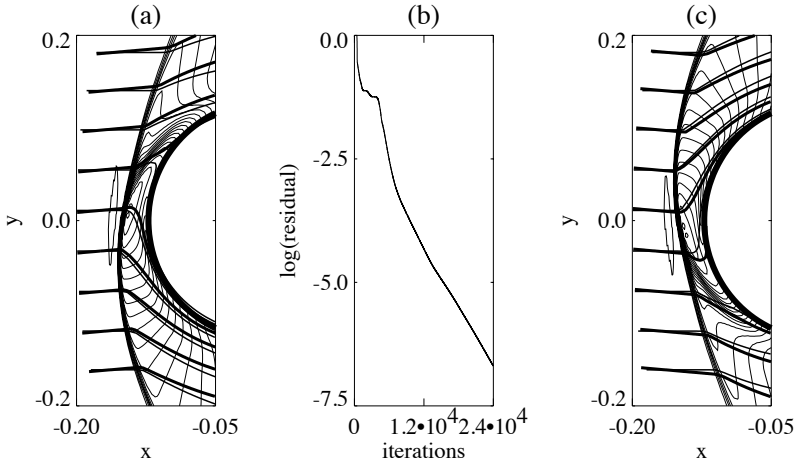

Figure 7.4: *Magnetically dominated 3D bow shock flows (switch-on shocks occur). (a) Density contours (thin solid) with streamlines (thick solid) and magnetic field lines (thin solid) in the xy plane for* $\theta_{vB} = 5°$. *This is the flow of Fig. 7.1. (b) Convergence of the density residual towards a steady state. (c) Bow shock flow for* $\theta_{vB} = -5°$ *(*$60 \times 60 \times 40$ *grid).*

We now consider bow shock flows with magnetically dominated upstream conditions, for which switch-on shocks occur. Fig. 7.4a shows the stationary simulation result for a bow shock flow with inflow parameters like for the flow of Fig. 7.3, except that we decrease the inflow velocity to $v = 1.5$. The simulations were performed on a $60 \times 60 \times 40$ grid with the second order LF scheme. With plasma $\beta = 0.4$ and Alfvénic

Mach number along the magnetic field lines M_{Ax}=1.49, Fig. 6.3a shows that switch-on shocks can exist, and the upstream flow is magnetically dominated. A 3D visualization of this flow was given in Fig. 7.1.

Fig. 7.4a shows that the geometry and topology of the magnetically dominated 3D bow shock flow is quite different from the topology of the pressure-dominated flow in Fig. 7.3. The shock front contains a slight dimple, and the leading front is followed by a secondary shock front. Fig. 7.4b shows that the simulation result converges to a perfect steady state. Fig. 7.4c shows that when the sign of the angle between the velocity and the magnetic field is changed ($\theta_{vB} = -5°$), the solution has the same topology but now with the secondary shock stretching out in the bottom part of the flow.

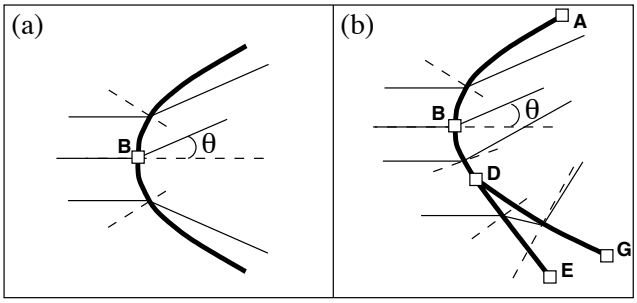

Figure 7.5: *(a) The shock front cannot entirely be of the 1–2 fast type in the neighborhood of a perpendicular point with a 1–2=3 switch-on shock. (b) A complex shock topology is necessary to channel the flow. Shock segment AB is of 1–2 fast type, BD is 1–3 intermediate, DE is 1–2 fast, and DG is 2–4 intermediate, evolving into 2=3–4 switch-off and 3–4 slow along the front. This shock topology is obtained in the numerical simulations of magnetically dominated 3D bow shock flows.*

We now investigate the topology of the magnetically dominated flow of Fig. 7.4c in the xy plane. Clearly only one perpendicular point is present in the xy plane, and the shock is a 1–2=3 switch-on shock at this point. The reasoning presented in Sec. 6.1 showed that for this case the topology represented in Fig. 6.4b (repeated in Fig. 7.5b) is needed to channel the flow. And indeed, inspection of the shock shapes in the flow of Fig. 7.4c indicates that we find exactly this topology! This is confirmed in the following paragraphs by identification of the types of all the shock segments in the simulation result. The shock segment above the 1–2=3 switch-on shock can be of 1–2 type, but the segment below the switch-on shock *cannot* be of 1–2 type (Fig. 7.5a). Instead, this shock segment has to be of 1–3 type. The curved 1–3 intermediate

shock segment BD can only have a limited extent, however, because for increasing angle between the magnetic field and the shock normal, the 1–3 shock first becomes a 1–3=4 shock and then ceases to exist (Fig. 3.9). At this point the leading shock front splits up into two consecutive shock fronts. The leading shock segment DE is of the 1–2 fast type, and the secondary shock segment DG is 2–4 intermediate. The combination of the fast and the intermediate shock can deflect the magnetic field such that field lines merge continuously downstream of the so-called λ-point D where the three shock segments meet.

In the case of 2D field-aligned flow (Fig. 6.2), symmetry imposes extra constraints on the solution which makes that three perpendicular points arise in a complex flow topology, with the topology of Fig. 7.5b arising locally at several places along the leading shock front. In the 3D case, however, no extra symmetry constraints are imposed and the topology of Fig. 7.5b applies directly to the bow shock flow in the plane of symmetry (xy). The solutions of Fig. 7.4 are clearly far from being axi-symmetrical. The question thus arises what is the spatial form and extent of the secondary shock front away from the xy plane. Fig. 7.1 gives a good idea of this extent. We postpone further discussion of the 3D topology away from the xy plane to Sec. 7.3.

It is interesting to examine the shock types and the location of the stagnation points in bow shock flows with the topology of Fig. 7.4. Fig. 7.6 shows a detailed representation of a 3D bow shock flow with inflow parameters $\rho = 1$, $p = 0.2$, $B_x = 1$, $B_y = 0$, $v_x = 1.5$ and $v_y = 0.1$. The angle θ_{vB} thus equals 3.8°. To obtain sufficient resolution we performed the simulation on a $60 \times 120 \times 60$ grid with Linde's second order HLLE scheme. The grid points are strongly clustered near the sphere. The velocity and magnetic stagnation points (the lower and the upper thick dots immediately in front of the sphere, respectively) are clearly separated and are located far above the horizontal line through the center of the sphere, even though the angle θ_{vB} is quite small in the upstream plasma.

It is conceivable that for larger angles θ_{vB} these stagnation points would shift away along the sphere even further. In that case, it would be difficult to simulate the flow on a domain restricted to one quadrant (the domain depicted in Fig. 7.2). For this reason we restrict ourselves to simulations of flows with small angles θ_{vB} in this Chapter. It seems that the structured grid approach adopted in our code is not ideally suited for the general problem of the flow around a sphere with arbitrary angle between the fields. Indeed, it is topologically difficult to fully cover a domain around a sphere by wrapping a logically rectangular box around it [155]. Adaptive or unstructured grid techniques would probably be more appropriate [56, 100, 167, 22]. On the other hand, it is not necessarily a good idea to consider the whole domain around

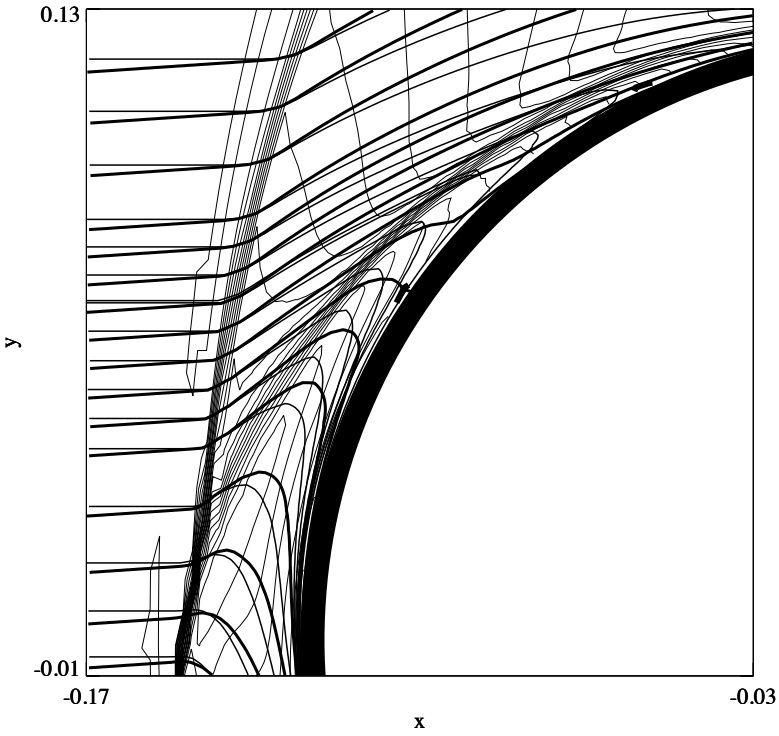

Figure 7.6: *Detailed representation of a magnetically dominated 3D bow shock flow. Density contours (thin solid) with streamlines (thick solid) and magnetic field lines (thin solid) are shown in the xy plane. The two thick dots immediately in front of the sphere indicate the location of the velocity and magnetic field stagnation points* ($60 \times 120 \times 60$ *grid).*

the sphere in simulations, because simulation of the wake region on the backside of an obstacle (e.g. Fig. 6.30) requires a high spatial resolution, which would necessitate excessive computing resources in the case of 3D problems. In the next Chapter we consider 3D MHD bow shock flows around a perfectly conducting paraboloid surface. Wake flows are largely avoided in this configuration, although boundary layer separation can occur. In the next Chapter we consider large angles θ_{vB} for this flow configuration with a paraboloid surface, and also for magnetically dominated bow shock flows with large angles θ_{vB} we consistently obtain

the topology of Fig. 7.5b.

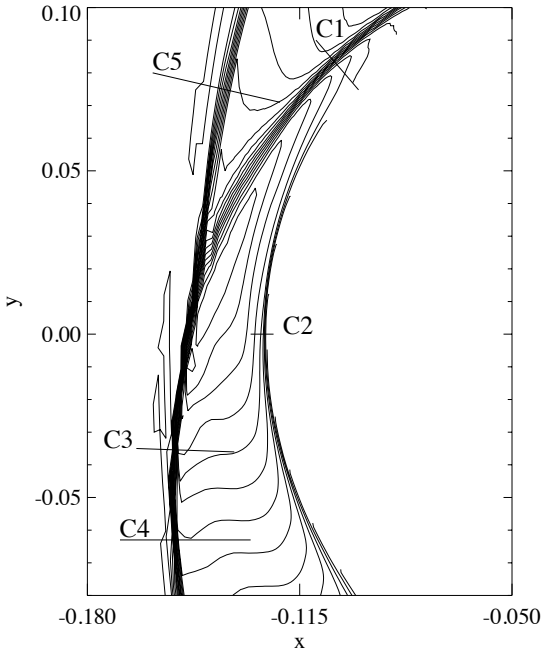

Figure 7.7: *Cuts perpendicular to various shock fronts.*

In Fig. 7.7 we indicate cuts perpendicular to various shock fronts which are now used to determine shock types for the flow of Fig. 7.6.

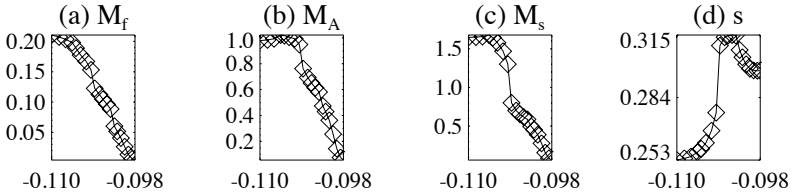

Figure 7.8: *Cut along C1 perpendicular to the secondary shock front in Fig. 7.7.*

Fig. 7.8 shows plots of Mach numbers and entropy along the cut C1 perpendicular to the secondary shock in Fig. 7.7. We see that the

upstream Alfvénic Mach number is slightly larger than one, and the slow Mach number jumps from above one to below one. This shock is thus a 2–4 intermediate shock, which is very close to a 2=3–4 slow switch-off shock. This shock is of the same type as shock part D–G–H–I in the symmetrical 2D bow shock flow (Figs. 6.7 and 6.9), and as the secondary shock in the non-symmetrical 2D solution of Fig. 6.31.

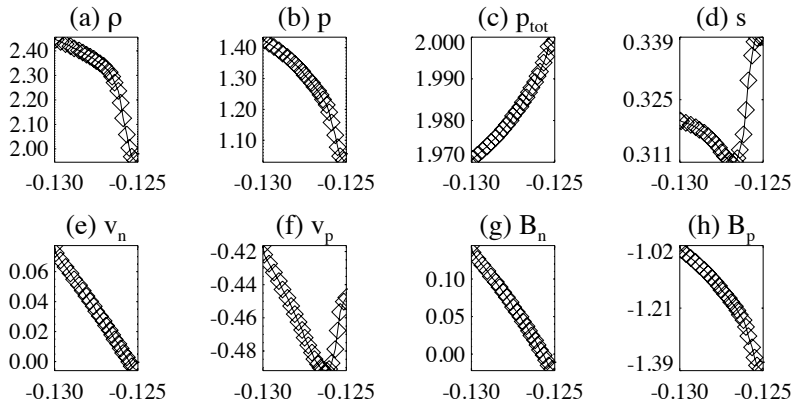

Figure 7.9: *Cut along C2 in Fig. 7.7.*

Fig. 7.9 shows plots of various quantities along the cut C2 in Fig. 7.7. Near the sphere some kind of *boundary layer* seems to be present. Such a boundary layer seems not to be present in the flow of Fig. 7.3 for pressure-dominated parameters. It is difficult to assert if this boundary layer is of physical nature or a numerical artefact. It may be a relevant part of the ideal MHD flow topology, or it may be a dissipative boundary layer, with the numerical dissipation playing the role of physical dissipation. The plots in Fig. 7.9 show some evidence that this boundary layer may be separated from the rest of the flow by a tangential discontinuity. Indeed, the normal velocity and magnetic field seem to vanish where the thermodynamic variables and the tangential fields make a jump. The total pressure does not make a noticeable jump. It seems that simulations with higher resolution are necessary to allow a more definite interpretation.

Figs. 7.10–7.12 show plots of Mach numbers and entropy along the cuts C3, C4 and C5 perpendicular to the leading shock front in Fig. 7.7. At cut C3 the shock is of the 1–3 intermediate type, but very close to 1–3=4. At cut C4, near the 'nose' of the bow shock, the shock is very close to a 1–2=3 fast switch-on shock. At cut C5, the shock is of the 1–2 fast type.

Fig. 7.13 shows that for the upstream parameter values of Fig. 7.6

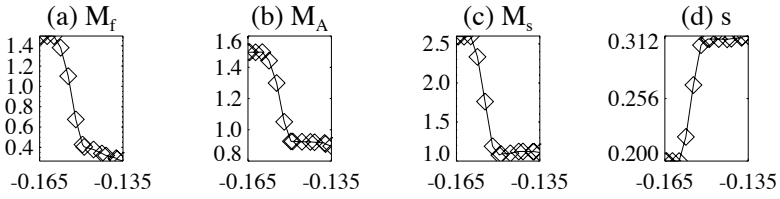

Figure 7.10: *Cut along C3 through the leading shock front in Fig. 7.7.*

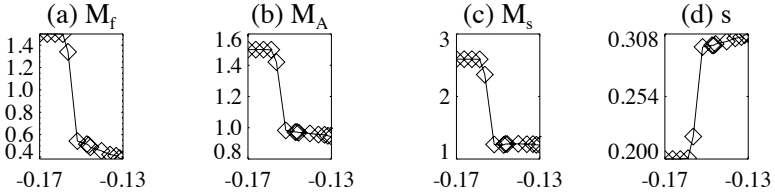

Figure 7.11: *Cut along C4 through the leading shock front in Fig. 7.7.*

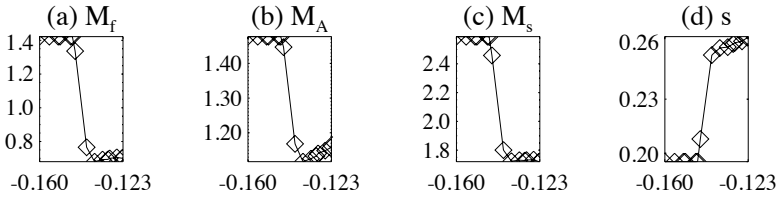

Figure 7.12: *Cut along C5 through the leading shock front in Fig. 7.7.*

the maximum angle between the magnetic field and the shock normal for which the 1–3 intermediate shock can occur is approximately 3°. This is consistent with the angle for which the leading shock front splits up into two consecutive shock fronts in Fig. 7.7.

Fig. 7.14 shows how magnetic field lines (black) and streamlines (blue) originating from points located slightly above the xy plane drape around the sphere for the bow shock flow solution of Fig. 7.1. The way in which field lines drape around obstacles is important in many space physics bow shock flows because field line orientation influences important physical processes like reconnection. This is discussed in the next Chapter. It is obvious that field line draping in the new magnetically dominated bow shock topology is quite different from field line draping

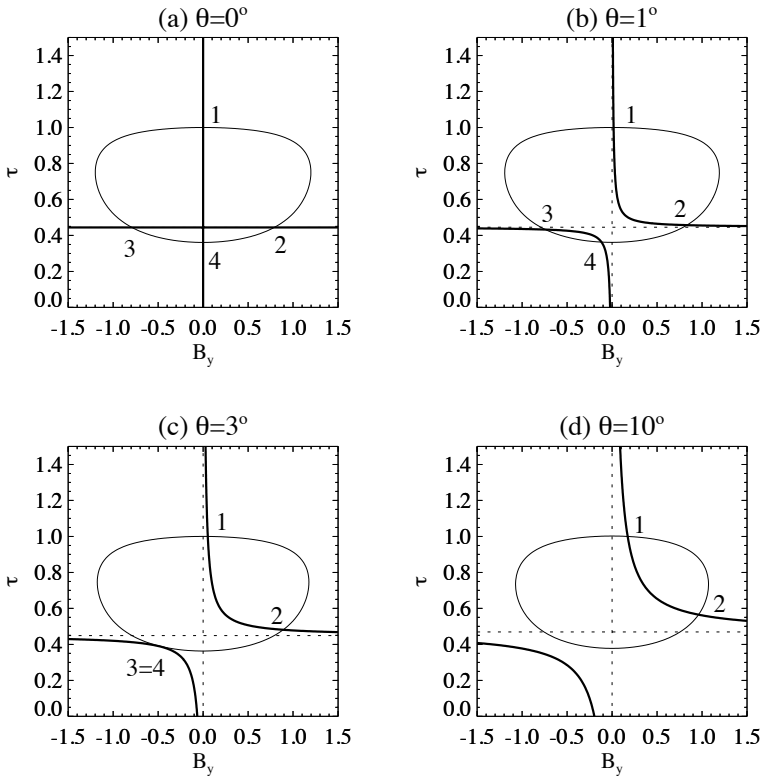

Figure 7.13: *Solutions of the RH relations for the upstream parameters of Fig. 7.6 with* $\theta_{vB} = 3.8°$. *These parameters are magnetically dominated. The maximum angle between the magnetic field and the shock normal for which intermediate shocks can occur is approximately* 3°.

in the traditional pressure-dominated MHD bow shock flows, since magnetic field lines undergo a strong secondary refraction at the secondary shock, as can be seen in Figs. 7.14 and 7.1.

The results presented in this Section show that there are two basic topologies for 3D MHD bow shock flows. For pressure-dominated upstream flows a single-front topology is obtained which is the same as the well-known topology of hydrodynamic bow shock flows. For magnetically dominated upstream flows, we find the complex bow shock topology sketched in Fig. 7.5b.

The conclusion on 3D MHD bow shock topology formulated above is

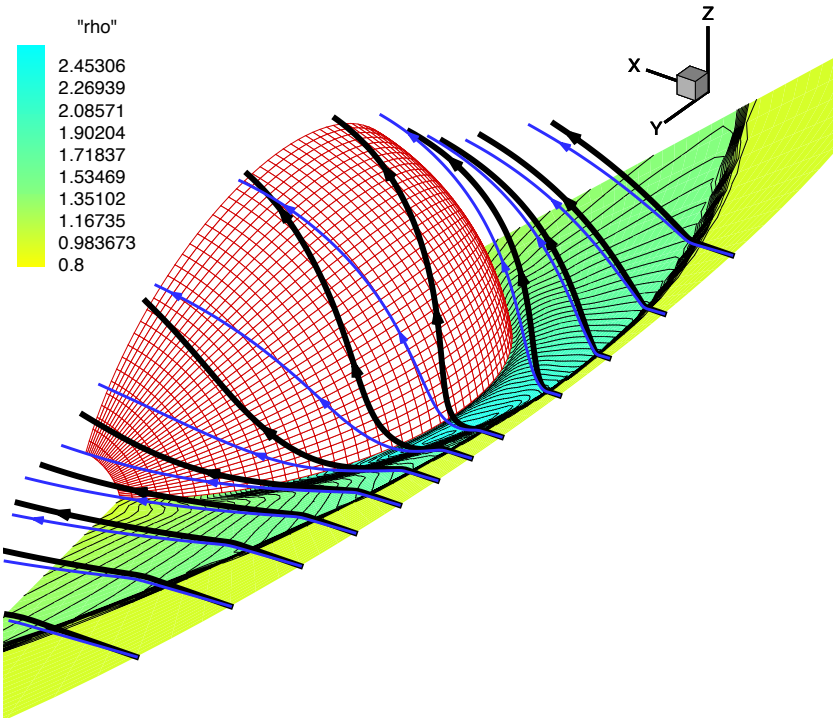

Figure 7.14: *Magnetic field lines (black) and streamlines (blue) for the bow shock flow solution of Fig. 7.1. The field lines and streamlines are drawn starting from points located slightly above the xy plane, and drape around the sphere.*

completely analogous to the conclusion reached for the case of symmetrical 2D flow (Sec. 6.3), and is a further justification for the terminology of magnetically dominated versus pressure-dominated upstream states, bow shock flows and bow shock flow topologies which we have been using since the Introductory Chapter.

We have to qualify the above formulated conclusion in the following way. Due to limited computer resources, we have not performed a complete parameter study for the 3D flows as we have done for the 2D flows (Sec. 6.3). Also, simulations were limited to small angles θ_{vB} because of limitations of the numerical technique. Nevertheless, we have simulated substantial numbers of flows around a sphere with both pressure-dominated and magnetically dominated upstream conditions. In all cases we have obtained the single-front topology for pressure-dominated up-

stream flows, and the multiple-front topology for magnetically dominated upstream flows. Combined with the theoretical reasoning leading to the topology of Fig. 7.5b for magnetically dominated upstream conditions, these results are a strong indication that the two different topologies indeed arise for the two different types of upstream conditions. In this context we have to remark that the topology of 3D MHD bow shock flows can be complicated further by the appearance of additional slow and intermediate shocks in the downstream flow. These additional features, however, are not related to the geometrical properties of switch-on shocks at perpendicular points on the leading shock front, but instead seem to depend more on the shape of the obstacle and the angle θ_{vB} and can be the result of other physical processes like boundary layer separation. Some examples of such additional features are given in the next Chapter (Sec. 8.2.2).

7.2 Field-aligned axially symmetrical flow over a sphere

In the present Section the special case of axi-symmetrical 3D bow shock flow over a sphere with the magnetic field aligned to the flow ($\theta_{vB} \equiv 0$) is considered. We present numerical simulation results for magnetically dominated inflow parameter values $\beta = 0.4$ and $M_{Ax} = 1.5$ for which switch-on shocks occur (Fig. 6.3a). These are the same parameters as for the bow shock flow around a cylinder which was studied in Sec. 6.2. First we discuss the simulation results obtained with our 2D axi-symmetrical scheme, which was described in Sec. 4.2.4.

In Fig. 7.15b we show a global view of the stationary axi-symmetrical bow shock solution, obtained with our second-order LF scheme on a stretched 100×100 grid restricted to one quadrant. The horizontal x-axis (coinciding with the stagnation streamline) is an axis of rotational symmetry. At the symmetry axis no boundary conditions need to be specified because the effective length of the cell interfaces on the axis vanishes, such that the flux through these interfaces does not contribute to the time evolution. At the three other boundaries we impose standard free in, free out and ideal wall conditions. The leading shock front shows a clear dimple. The shock front is much closer to the obstacle than in the case of the flow around a cylinder with the same inflow parameters, which is shown in Fig. 7.15a for comparison.

In Fig. 7.15c we show a detailed representation of the central part of the axi-symmetrical bow shock solution near the stagnation streamline. This plot is to be compared to its cylinder flow equivalent shown in Fig. 6.9 (where only the upper part of the symmetrical flow is plotted). The flow clearly exhibits a topology which is similar to the topology of

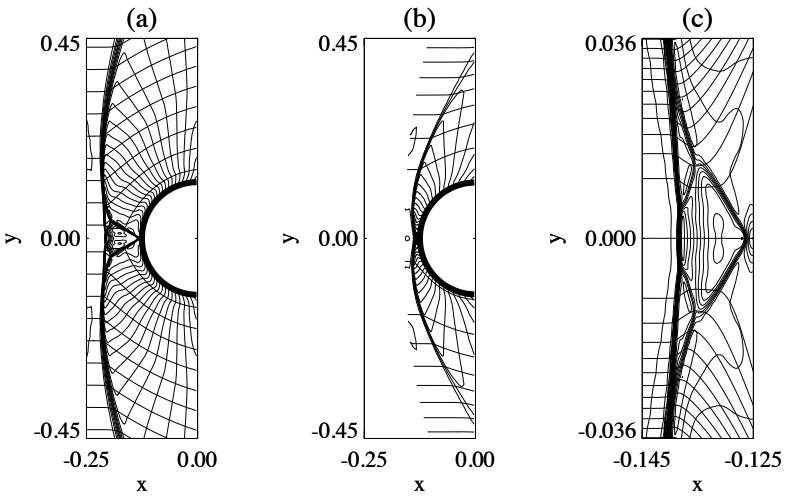

Figure 7.15: *Symmetrical field-aligned magnetically dominated bow shock flows with $M_A = 1.5$ and $\beta = 0.4$. Density contours and magnetic field lines are shown. (a) Flow around a cylinder. (b) Axi-symmetrical flow over a sphere. (c) Detail of the axi-symmetrical flow.*

the flow around a cylinder. Inspection of the way in which the field lines are refracted when the shocks are passed, reveals that the shocks in Fig. 7.15c are of the same type as the shocks in the cylinder flow of Fig. 6.9 which were discussed in Sec. 6.2, and detailed analysis of upstream and downstream Mach numbers, along the lines of the detailed analysis in the previous Chapter, confirms this conclusion.

We can thus conclude that magnetically dominated 3D axi-symmetrical flows over a sphere exhibit a complex bow shock topology very similar to the topology of a bow shock flow around a cylinder in that parameter regime.

The axi-symmetrical 3D flow over a sphere can of course also be simulated using our 3D simulation code, and the same result should be obtained as with the 2D axi-symmetrical code. In fact, comparison of the results constitutes a good test for the 3D code. Fig. 7.16 shows a comparison of simulation results for the axi-symmetrical bow shock flow obtained with the 3D code on a $50 \times 100 \times 50$ grid in the xy plane (solid) and in the xz plane (dashed), and the results obtained with the 2D axi-symmetrical code on a 80×80 grid (dotted). The results are in global agreement. The differences between the 2D and the 3D results are due

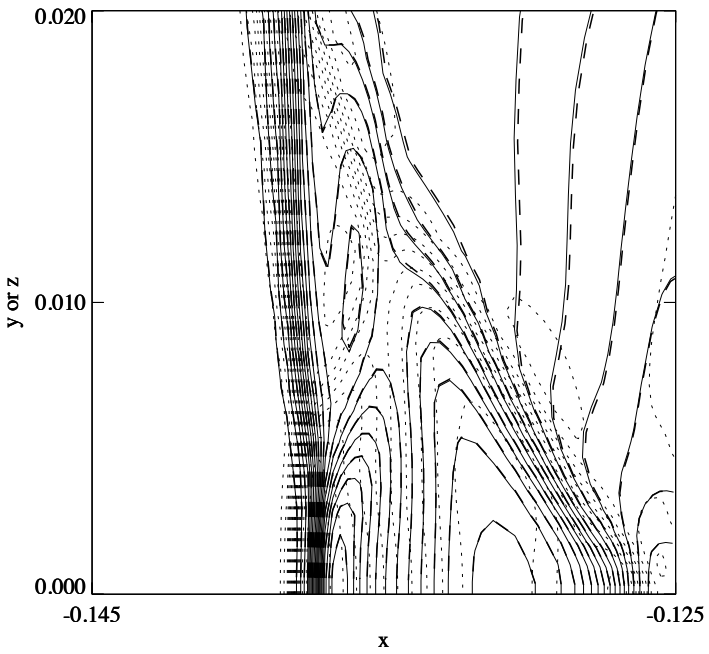

Figure 7.16: *Comparison of simulation results for the axi-symmetrical flow obtained with the 3D code in the xy plane (solid) and in the xz plane (dashed), and the results obtained with the 2D axi-symmetrical code (dotted).*

to the difference in grid resolution and structure.

The topology of the flow in Fig. 7.4a for $\theta_{vB} = 5°$ is very different from the solution for the axi-symmetrical field-aligned case which was shown in Figs. 7.15b and c, even though the angle $\theta_{vB} = 5°$ in Fig. 7.4a is quite small. We have performed simulations for even smaller but non-vanishing angles θ_{vB} between the inflow velocity and magnetic field. In all cases we find the topology of Fig. 7.4a for the stationary solution, and not the topology of the axi-symmetrical solution of Fig. 7.15c, which corresponds to the sketch in Fig. 6.7. This seems to be a clear example of symmetry breaking, because introduction of a small

angle θ_{vB} between the magnetic field and the plasma flow, produces a steady state result which is topologically different from the symmetrical solution. The symmetrical flow is thus likely to be a meta-stable solution. This conclusion is consistent with the results of the discussion in Sec. 6.5 about the stability of the symmetrical 2D bow shock flow. In Sec. 7.4 it is discussed how transient waves form the link between the symmetrical and non-symmetrical flow solutions.

7.3 3D topology of magnetically dominated bow shock flows

As shown in Sec. 7.1.3, the reasoning leading to Fig. 7.5b explains the topology of 3D magnetically dominated bow shock flows in the plane of symmetry. However, the topology of the flow away from the xy plane remains to be investigated and explained. Fig. 7.1 shows that the secondary shock has a finite extent out of the plane of symmetry. We now investigate if this can be understood in terms of the properties of MHD shocks. First we study the local geometry of 3D MHD shock fronts near perpendicular points for magnetically dominated upstream parameters (switch-on shocks occur). For simplicity we consider again the case of a uniform upstream flow, but the upstream velocity and magnetic field need not be aligned.

Let us first consider the possible existence of an isolated perpendicular point at the nose of a fast MHD shock front with concave-inward orientation (Figs. 7.17a and b). The shock at the perpendicular point can either be a fast 1–2=3 switch-on shock or a 1–4 hydrodynamic shock. Suppose that the shock is a switch-on shock, as in Fig. 7.17a. Suppose that the magnetic field line is deflected leftward in the horizontal plane. The shock in the horizontal plane (thick solid) then necessarily has to be 1–2 on the left side, and a 1–3 shock segment can continuously be connected to the perpendicular point on the right, as in the 2D case of Fig. 6.5a. However, the shock segment in the vertical plane (thick dashed) cannot be connected continuously to the switch-on shock at the perpendicular point, because due to the co-planarity of MHD shocks the refracted magnetic field has to lie in the vertical plane containing the shock segment! This leads us to the conjecture that, for upstream parameters in the switch-on regime, isolated perpendicular points of switch-on type cannot exist on concave-inward shock fronts. The same conclusion seems to hold for concave-outward shock fronts (corresponding to the case of Fig. 6.5b).

If the shock at the perpendicular point is a hydrodynamic shock, as in Fig. 7.17b, then a concave-inward or concave-outward shock surface entirely of 1–4 type can exist with the isolated perpendicular point at

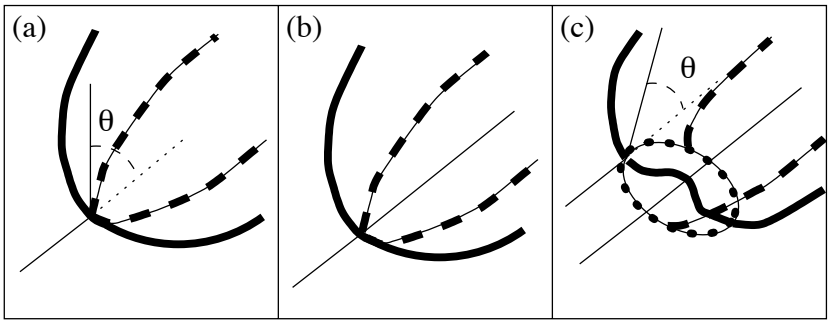

Figure 7.17: *3D bow shock geometries near perpendicular points for magnetically dominated upstream parameters. Thin lines are magnetic field lines. Shock fronts in the horizontal plane through the central perpendicular point are thick solid, and shock fronts are thick dashed in the vertical plane through the central perpendicular point which contains the incoming magnetic field line. (a) An isolated perpendicular point of 1–2=3 switch-on type cannot exist. (b) An isolated perpendicular point of 1–4 hydrodynamic type can exist. (c) A closed curve of perpendicular points of switch-on type (thick dotted) forms the transition between a 1–2 shock front on the outside and a central concave-outward dimple containing 1–3 and 1–4 shocks.*

the nose (corresponding to the cases of Figs. 6.5e and f).

However, 1–2 fast MHD shock fronts certainly exist in 3D MHD flows with magnetically dominated upstream parameters, so what happens if a 1–2 front assumes a shape such that the magnetic field becomes perpendicular to the 1–2 front at some point on the shock surface, where the fast shock then would turn into a switch-on shock? The reasoning described above shows that isolated perpendicular points are not possible in this case, but it seems that *continuous curves* of perpendicular points with switch-on shocks can exist on the shock front. Fig. 7.17c shows a possible symmetrical 3D shock geometry for the case of magnetically dominated upstream parameters. The shock front contains a concave-outward central part or 'dimple'. The central part of the dimple is of 1–4 type, and contains a perpendicular point of hydrodynamic type. A closed circular curve exists on the shock front at which the shock is of 1–2=3 switch-on type (thick dotted). Outside of this curve the shock front is of 1–2 type, and on the inside the shock is 1–3. This shock geometry is a direct 3D generalization of the geometry proposed by Steinolfson and Hundhausen for 2D flows (Fig. 6.6b). The simulation of a symmetrical field-aligned flow over a sphere represented in Fig. 7.15 shows that, like

in the case of 2D flow around a cylinder, the single-front topology with a dimple which was proposed in Fig. 7.17c does not occur. Instead, the 1–3 and 1–4 shock segments split up into two consecutive shock fronts at the points where the shocks become 1–3=4.

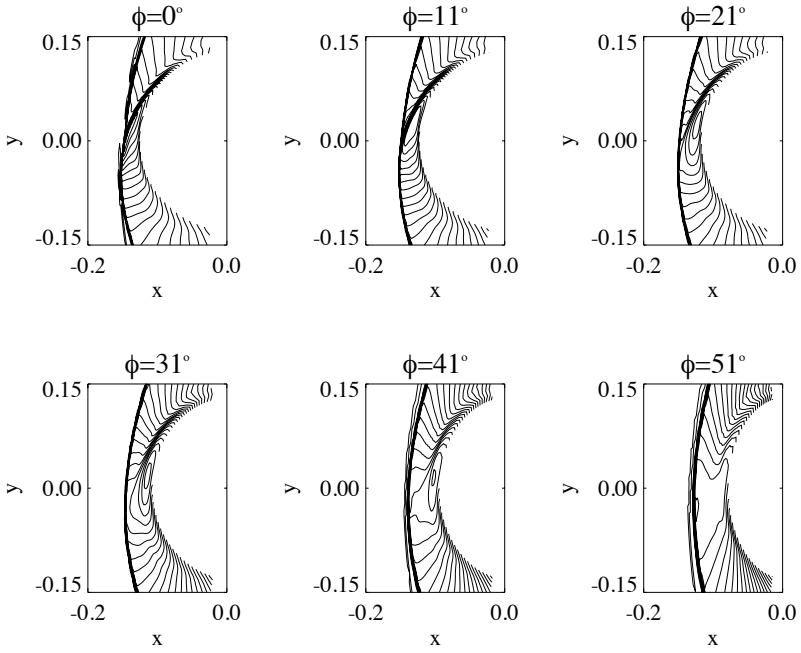

Figure 7.18: *The 3D bow shock flow of Fig. 7.1 in planes with various values of ϕ. Density contours in those planes are projected on the xy plane.*

For non-vanishing upstream angle θ_{vB}, the flow solution becomes highly non-symmetrical, and the flow topology changes accordingly. Fig. 7.4a shows that there is only one perpendicular point on the leading front in the xy plane. The question thus arises what is the spatial form and extent of the secondary shock front away from the xy plane, and how this is related to the flow topology. Fig. 7.1 gives some indication about the extent of the secondary shock.

Fig. 7.18 gives some more information about the precise flow topology. The secondary shock front remains attached to the leading front up to an angle of $\phi \approx 20°$. For higher values of ϕ the secondary shock is detached from the leading front. It is interesting to remark that the perpendicular point (at the nose) remains approximately at the same x

location for ϕ between 0° and approximately 20°. For ϕ increasing from 0° to approximately 20°, the perpendicular point seems to approach the point where the secondary shock is attached to the leading front. We propose the following possible interpretation for this behavior.

In Fig. 7.4a we see that a switch-on shock is present on the leading shock front at the perpendicular 'nose' point, where the shock front extends most into the undisturbed upstream plasma. The magnetic field is deflected downwards at this point. The above discussion indicates that this perpendicular point of switch-on type cannot be an isolated perpendicular point, which implies that a line of perpendicular points of switch-on type has to extend in two directions out of the xy plane and perpendicular to that plane. In the topology of Fig. 7.4a, this curve of perpendicular points on the leading shock front can clearly not be a closed curve. It is conceivable that this curve of perpendicular points would end when it connects to the secondary shock at some point on the leading front above the xy plane. Fig. 7.18 seems to suggest that this happens for an angle $\phi \approx 20°$. For higher values of ϕ both the secondary shock and the switch-on shock are not present anymore on the leading shock front. Perpendicular points of switch-on type thus exist on the leading front up to a value of $\phi \approx 20°$. Beyond this value, the leading front curves away and perpendicular points do not occur anymore. This would explain how the secondary shock has a limited extent out of the xy plane. This seems to be a reasonable interpretation for this aspect of the complex bow shock flow topology, but thorough study of high resolution simulation results is needed to confirm this interpretation.

7.4 Transient waves during the time evolution towards a steady state

The V-shaped secondary feature composed of intermediate and compound shocks which is present in the axi-symmetrical flow result of Fig. 7.15c is clearly not present in the stationary bow shock results of Fig. 7.4 for the case of a small angle θ_{vB} between the velocity and the magnetic field. The final stationary results thus differ substantially, and we have used the term symmetry breaking to refer to this phenomenon. The reader may wonder why the V-shaped feature is not present in the solution, even when the angle θ_{vB} is very small. It is interesting to look in detail at the dynamical time evolution of the flow towards a steady state solution. We show that transient waves provide a link between the symmetrical and non-symmetrical magnetically dominated bow shock topologies. Indeed, in our simulations the uniform initial conditions for field-aligned flow and for flow with a small angle θ_{vB} are very close to each other, so we can expect that the resulting flow patterns do not differ

too much for small times. Let us examine the dynamical time evolution of symmetrical and non-symmetrical flows towards a steady state bow shock solution starting from a uniform initial condition.

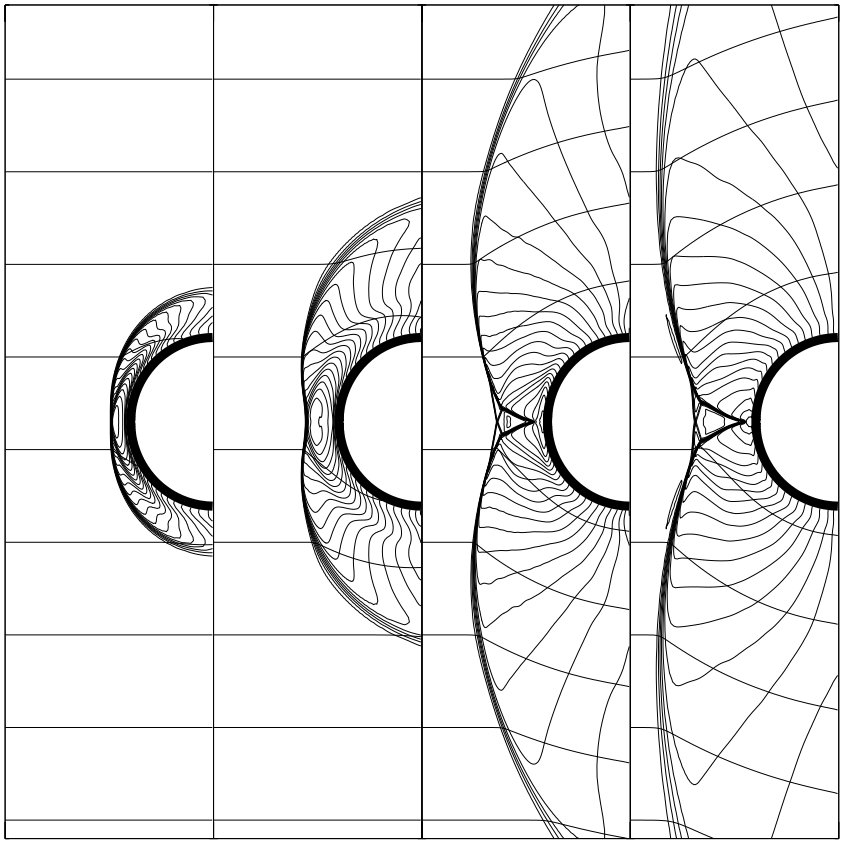

Figure 7.19: *Time evolution towards a steady state solution for the case of 2D magnetically dominated symmetrical flow around a cylinder. Density contours and magnetic field lines are shown (*200×400 *grid).*

Fig. 7.19 shows the time evolution towards a steady state solution for the case of 2D symmetrical flow around a cylinder, with $\beta = 0.4$ and $M_{Ax} = 1.2$ ($\rho = 1$, $p = 0.2$, $B_x = 1$, $v_x = 1.2$ and $r = 0.125$). The initially almost circular front ($t = 0.05$, first panel) deforms into a front composed of fast and intermediate shock parts, characterized by a concave-outward central part (the 'dimple') ($t = 0.15$, second panel). We also see traces of transient secondary shocks following the leading front. These transient features were also present in the time-dependent

CME simulations of Steinolfson and Hundhausen [147]. The shock on the stagnation line necessarily has to be a 1–4 intermediate shock. We propose as a possible explanation for these secondary shocks that at the point where the curving 1–4 shock becomes a 1–3=4 shock, the leading shock front splits up into two consecutive shock fronts.

At $t = 0.60$ (third panel), a V-shaped secondary shock front is seen to have separated from the leading shock front. It trails the leading front in a distinct V-shape, and the density is clearly depleted in the V-region ($\rho \approx 2$) as compared to the density in the two distinct lobes downstream of the slow shock front ($\rho \approx 3$). This V-shaped structure already has the topology of the steady symmetrical solution.

At $t = 1.00$ (fourth panel), the steady state is almost reached. Fig. 3.9 shows that for the parameter values of this flow the maximum angle between the magnetic field and the shock normal for which the 1–3 intermediate shock can occur is approximately 16°. This is consistent with the angle for which the leading shock front splits up into two consecutive shock fronts in the fourth panel of Fig. 7.19.

It may be argued that this time evolution starting from a uniform initial condition is somewhat artificial. We could propose the instantaneous acceleration of an object in a static uniform plasma to a constant velocity as a physical interpretation for such time-dependent flows, and this scenario can be approached in physical systems. We solve the time-dependent ideal MHD equations in a time-accurate way, and all the transient wave phenomena observed in the simulations are thus valid dynamical MHD phenomena. These phenomena may be of real physical interest, maybe not directly in the abstract setting of the problem we simulate, but possibly in related real plasma flows.

Fig. 7.20 shows a detailed representation of a snapshot ($t = 0.3$) of the evolution towards a steady state 3D bow shock flow with inflow parameters $\rho = 1$, $p = 0.2$, $B_x = 1$, $B_y = 0.01$, $v_x = 1.5$, $v_y = 0$ and $r = 0.125$. The angle $\theta_{vB} = -0.57°$. The Alfvénic Mach number along the magnetic field line equals 1.4999, and $\beta = 0.4$. To obtain sufficient resolution we performed the simulation on a $60 \times 120 \times 60$ grid with Linde's second order HLLE scheme.

The final stationary solution of this flow problem has the topology of Fig. 7.4c, with the secondary shock front stretching out along the sphere in the bottom part of the flow. We see that in the initial stage of the evolution shown in Fig. 7.20 a clear V-shaped secondary shock feature is present in the flow. Detailed analysis shows that this V-shaped feature has the same topology as the V-shaped feature of the stationary axisymmetrical flow in Fig. 7.15c, although its proportions are different and its shape is non-symmetrical. The upper triangle D–G–E of Fig. 6.7 is much larger in this non-symmetrical flow, and the corresponding lower triangle is so small that it hardly can be identified. At this stage of

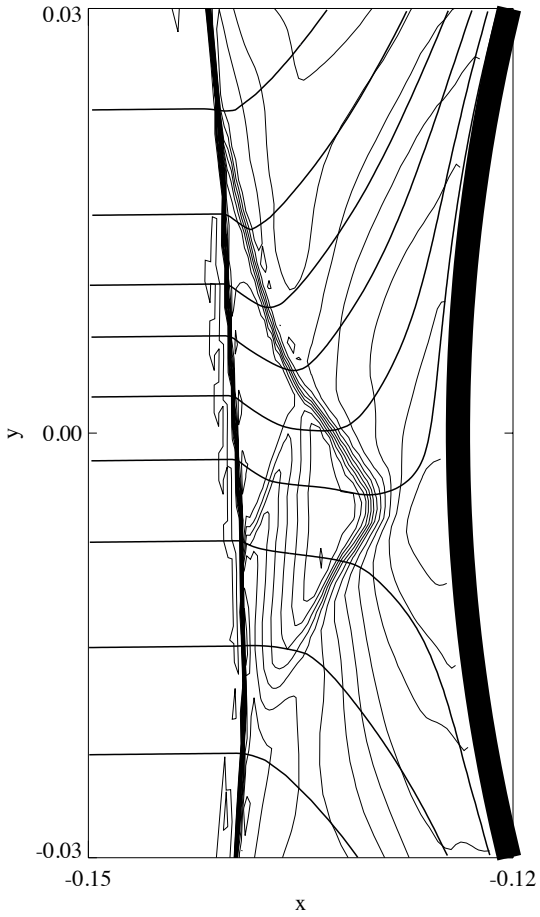

Figure 7.20: *Detailed representation of a snapshot ($t = 0.3$) of the evolution towards a steady state 3D magnetically dominated bow shock flow with non-field-aligned inflow. Density contours and magnetic field lines in the xy plane are shown ($60 \times 120 \times 60$ grid).*

the flow there are *three* perpendicular points on the leading shock front — the 1–4 point can be identified in the region plotted; the two 1–2=3 points lie above and below the plotted region. It is especially noteworthy that the 1=2–3=4 compound shock (E–G in Fig. 6.7, clearly visible in the upper triangle), is present in these 3D simulation results.

Later in the time evolution the V-shaped feature slips away along the sphere on the bottom side, and disappears completely. The remaining secondary shock (like in Fig. 7.4c) can be identified with the shock D–G–H–I in the V-shaped feature (they are both of 2–4 type), and is the sole remainder of the V-shaped feature in the stationary bow shock solution. In the final solution there is only one perpendicular point.

When the incoming magnetic field is aligned to the flow, the V-shaped feature is not biased to slip away on the top or the bottom side, and consequently it reaches a stationary position in front of the sphere. For small angles θ_{vB}, however, the V-shaped feature finds a way to slip around the sphere. This explains why the symmetrical solution with a stationary V-shaped feature is likely to be a meta-stable solution. The important conclusion from the analysis in this Section is that the V-shaped feature with all its constituting intermediate and compound shocks can be present in non-field-aligned 3D bow shock flows as a transient feature.

7.5 Conclusion

The main lesson to be learned from the results described in this Chapter is that there are two basic topologies for 3D MHD bow shock flows. For pressure-dominated upstream flows a single-front topology is obtained which is the same as the well-known topology of hydrodynamic bow shock flows. For magnetically dominated upstream flows we find the complex bow shock topology sketched in Fig. 7.5b. The complexity of the magnetically dominated MHD bow shock topology is due to intrinsically magnetic effects. It was previously thought that all MHD bow shock flows exhibit the traditional pressure-dominated topology, and the magnetically dominated MHD bow shock topology was unknown. The new magnetically dominated MHD bow shock topology has important applications in space physics plasma flows, which are discussed in the next Chapter.